# Preparation of plasmonically resonant VO₂ thermochromic pigment

Huaping Bai[1,2], Michael B Cortie[2], Abbas I Maaroof[2], Annette Dowd[2], Catherine Kealley[2] and Geoffrey B Smith[2]

[1]Nanjing University of Science and Technology, Nanjing, 210094 (China)

[2]University of Technology Sydney, PO Box 123, Broadway NSW 2007 (Australia)

E-mail: michael.cortie@uts.edu.au

PACS : 78.20.Bh, 78.20.Nv, 78.30.-j, 78.67.Bf

Short title :Plasmonically resonant VO₂ pigments

## Abstract

Vanadium dioxide (VO₂) undergoes a reversible metal-insulator transition, normally at ~68˚C. While the properties of continuous semi-transparent coatings of VO₂ are well known, there is far less information available concerning the potential use of discrete VO₂ nanoparticles as a thermochromic pigment in opaque coatings. Individual VO₂ nanoparticles undergo a localized plasmon resonance with near-infrared light at about 1100 nm and this resonance can be switched on and off by simply varying the temperature of the system. Therefore, incorporation of VO₂ nanoparticles into a coating system imbues the coating with the ability to self-adaptively modulate its own absorptive efficiency in the near-infrared. Here we examine the magnitude and control of this phenomenon. Prototype coatings are described, made using VO₂ powder produced by an improved process. The materials are characterized using calorimetry, X-ray diffraction, hi-resolution scanning electron microscopy, transmission electron microscopy, and by measurement of optical properties.

## 1. Introduction

Vanadium forms a variety of binary oxides, examples of which include $V_2O_5$, $V_3O_7$, $V_6O_{13}$, $VO_2$, $V_6O_{11}$, $V_4O_7$, $V_2O_3$, and various hydrated compounds, e.g. $VO_2.nH_2O$ [1]. These materials have potential or actual applications as catalysts, chemical sensors, electrodes and as the active components of various electrical and optical devices [2, 3]. Two of the four polymorphs[4] of vanadium dioxide ($VO_2$) have the unusual attribute of undergoing a mutual and reversible metal/insulator phase transition [5]. This transition, which evidently occurs by a displacive transformation between the tetragonal (rutile structure) $VO_2$-R and monoclinic $VO_2$-$M_1$ phases, is accompanied by significant changes in the optical properties, particularly in the infrared region of the spectrum [6]. For this reason $VO_2$ has been considered for use as a 'smart' coating on glass or for use in optical switches [3, 6-14]. The transformation occurs at about 68°C in pure material, with some hysteresis dependent on sample microstructure. The temperature of transition can be reduced somewhat by doping the $VO_2$ with W, Nb or Mo but this is accompanied by a reduction in the enthalpy of the transformation and a loss in the magnitude of change in the optical and electrical properties [1, 7, 10, 15]. The metallic $VO_2$-R is the high temperature phase, while $VO_2$-$M_1$ is a semi-conductor with a band gap of about 0.6 eV [16].

Modulation of the *transmission* of light by thin continuous films of $VO_2$ [8, 9, 17-19] or by coatings of $VO_2$ nanoparticles [7, 20-22] has previously attracted the bulk of the attention in this field. In contrast, there have been fewer investigations [7, 23-25] into the use of $VO_2$ particles as opaque pigments in thermochromic paint systems. We will show here that the localized plasmon resonance of metallic $VO_2$ nanoparticles becomes the controlling factor in this case. The fact that $VO_2$ and its nanoparticles can undergo a plasmon resonance with light is already known [21, 22, 26-29] but the role of the resonance in thermochromic paints has not been previously investigated. Such a coating system constitutes the basis of a 'smart' paint: one that can self-adaptively modulate its own absorptive efficiency in the near-infrared by switching localized surface plasmons on or off as the temperature is varied through the metal/insulator phase transition of the pigment. In particular we will address and

answer the following questions: to what extent is the intensity and position of the plasmon resonance of $VO_2$ nanoparticles in a such a 'paint' controlled by particle size, shape and packing, what should the particle morphology and concentration be to optimize the switchable effect and, finally, is the effect likely to be big enough to be technologically useful?

To undertake the experimental component of this research we required a supply of nanocrystalline $VO_2$. While there are many known methods by which $VO_2$ can be produced, including physical vapor deposition, aqueous reduction, ion implantation, chemical vapor deposition, and sol-gel processing [6], for the present work we sought an method based on aqueous chemistry. Such methods commonly begin with the reductive-precipitation of the metastable phases $VO_2.nH_2O$, $VO_2$-A or $VO_2$-B from some soluble vanadium precursor solution, followed by the conversion of the precipitated material to $VO_2$-R by calcination [2, 30]. In this case we used ammonium metavanadate ($NH_4VO_3$) solution as our source of V, and $KBH_4$ as reductant. The incorporation of small quantities of glycerol into the reactant mixture greatly improved the yield and reproducibility of the synthesis. Doping with Mo or W could be achieved by adding soluble salts of these elements to the $NH_4VO_3$ starting solution.

## 2. Experimental details

*Materials*. Ammonium metavanadate ($NH_4VO_3$), glycerol (analytical grade) and sodium molybdate ($Na_2MoO_4.2H_2O$) were purchased from Ajax Chemicals Ltd, Sydney, Australia. Potassium borohydride ($KBH_4$) was purchased from Sigma Chemical Co., hydrochloric acid (37% HCl) was obtained from Labscan Asia Co., Ltd, and sodium tungstate ($Na_2WO_4.2H_2O$) from M&B Ltd. Dagenham, England. All reagents were used without further purification.

The reaction can be written as :

$$6VO_3^- + BH_4^- + nH_2O \rightarrow 6VO_2.nH_2O(s) + BO_2^- + 4OH^- \qquad (1)$$
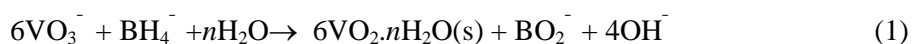
The VO$_2$.$n$H$_2$O is either amorphous or nanocrystalline after Reaction (1) - in either event it lacks an XRD pattern. During calcination the VO$_2$ may or may not [4] pass through the metastable VO$_2$-A and VO$_2$-B polymorphs en route to being converted to VO$_2$-R.

We found 0.20 to 0.25M NH$_4$VO$_3$ and KBH$_4$ to be convenient concentrations for our stock solution, although other concentrations were also used at times. The clear, yellow stock solution of NH$_4$VO$_3$ was obtained by dissolving weighed quantities of the salt in MilliQ water at ~80˚C. The KBH$_4$ solution was freshly produced, as needed, by dissolving the compound in ice-cold MilliQ water. The temperature must be kept low to prevent hydrolysis of borohydride  ion.

*Procedure.* Up to 20% by volume of glycerol was added to the vanadate solution. Following this, concentrated HCl was added drop-wise into between 10 and 50 mL of the NH$_4$VO$_3$ solution to adjust its pH to a selected value between 4.0 and 6.5. The reducing power of KBH$_4$ increases with the decreasing of pH value of the medium, suggesting that it might be more effective at the lower end of the pH range [2]. The reduction reaction was then carried out at the desired pH by slowly adding the KBH$_4$ solution while continuing the drop-wise additions of HCl and simultaneously stirring. At the end of the reduction reaction, the brown-black precipitate of VO$_2$.$n$H$_2$O was collected by filtration, washed several times with a mixture of water and methanol, and dried at about 90 ˚C in an air oven. The dry solid is amorphous or at best nanocrystalline at this stage, in agreement with that produced in other wet chemical reductive schemes, e.g. [2]. This material can be converted to VO$_2$-R by calcination in an inert environment [2, 31].  In the present work we used an environment of argon or nitrogen. The gases used may have contained up to 20 ppm oxygen as an impurity. Finally, on reverting to room temperature, the VO$_2$-R transformed to VO$_2$-M$_1$ by the metal-to-insulator transition discussed earlier. Doping with Mo and W was achieved by adding a solution of the relevant salt (66 mg Na$_2$MoO$_4$ or 47 mg Na$_2$WO$_4$.2H$_2$O, both in 20 ml H$_2$O) into 40 ml of 0.25M NH$_4$VO$_3.$ These proportions were selected to give a nominal 3 wt.% of the dopant in the VO$_2$.

*Characterization*. The as-synthesized samples were analyzed by a combination of differential thermal analysis (DTA) and thermal-gravimetric analysis (TGA) in an SDT 2960 machine (TA Instruments Inc., U.S.A.) with a heating speed of 10˚C /min and in a flowing $N_2$ atmosphere. The phase transformation temperature in samples that had already been converted to $VO_2$-$M_1$ was determined by differential scanning calorimetry (DSC) in a DSC 2920 (TA Instruments Inc., U.S.A.). In this case the $VO_2$-$M_1$ was heated  from room temperature to 120 ˚C at 3˚C/min under a flowing air atmosphere, and then back to room temperature. Samples were also characterized by X-ray diffraction (XRD, Siemens D5000 Diffractometer) with Cu Kα radiation (λ=0.15406 nm). X-ray diffraction patterns were calculated from the published lattice data using the program Crystallographica[§]. Scanning electron microscopy (SEM) images were taken with a Zeiss Supra 55VP SEM. Energy dispersive spectroscopy (EDS) was conducted on a FEI XL 30 Environmental SEM. A standardless technique was used and oxygen obtained by difference. Samples for the transmission electron microscope (TEM) were prepared by allowing drops of an aqueous suspension of $VO_2$ powder to dry on a lacy carbon support. Due to the need to obtain electron transparency, the $VO_2$ particles examined in the TEM were not necessarily representative in size or thickness. Scattering and diffuse reflectance of opaque coatings of $VO_2$ powder on glass slides was determined in a custom-built spectrometer equipped with an integrating sphere. Light with wavelengths between 300 and 2000 nm was incident on the sample at 7º to the normal, and all scattered light was collected. Once again, a hot stage was used to vary the sample temperature.

*Calculations.* The light scattered off a $VO_2$ sphere can be calculated using the analytical solutions due originally to Mie [32]. Here we made use of the convenient utility 'MIEPlot', coded by P. Laven [33]. Optical properties of non-spherical nanoparticles and of agglomerates of particles were calculated using the discrete dipole approximation (DDA) code of Draine and Flatau [34, 35].  The refractive index data used was that of Verleur [36] which we confirmed in measurements of our own taken on thin films produced by physical vapor deposition. DDA calculations were run on targets rendered to about 24,000 dipoles, sufficient in this case to produce convergence.

---

[§]Crystallographica is produced by Oxford Cryosystems Ltd, of the United Kingdom.

## 3. Results

### 3.1 Variation of synthesis parameters in the absence of glycerol additions

*3.1.1 Aqueous reaction temperature.* None of the air-dried precipitates of $VO_2.nH_2O$ was crystalline, in agreement with the finding of Tsang for a similar system [2] and it was necessary to convert this amorphous material to $VO_2$-$M_1$ by heat treatment. Table 1 shows the effect of aqueous reaction temperature on the phase composition of the products *after* the sequence of precipitation, washing, air drying, calcination up to at least 600ºC and cooling to room temperature. The desired phase, $VO_2$-$M_1$ (JCPD card : 00-044-0252) was only formed when precipitation from the vanadate solution was performed at temperatures of 40˚C and below. However, these samples were also all contaminated with a small amount of the intercalation compound $\beta$-$K_xV_2O_5$, $x \approx 0.25$ (JCPD cards : 00-037-0070 and 00-039-0889). The potassium-containing impurity was also evident from EDS, (See Fig S1, Supporting Information). Some $V_6O_{13}$, another oxide of mixed valence, was also present in some samples. Neither $\beta$-$K_xV_2O_5$ or $V_6O_{13}$ undergo the metal-insulator transition and are therefore not desired in the present work. It can be seen that an increased temperature of reaction is not useful for synthesis of $VO_2$. This may be because the $KBH_4$ hydrolyzed more readily when it was dropped into the warmer reaction solution, with a consequent reduction in reductive efficacy. It was found that $\beta$-$K_xV_2O_5$ could be removed from the precipitate by thorough washing with a mixture of warm water and methanol. A representative X-ray diffraction pattern for pure $VO_2$-$M_1$ prepared by this route is provided in figure 1.
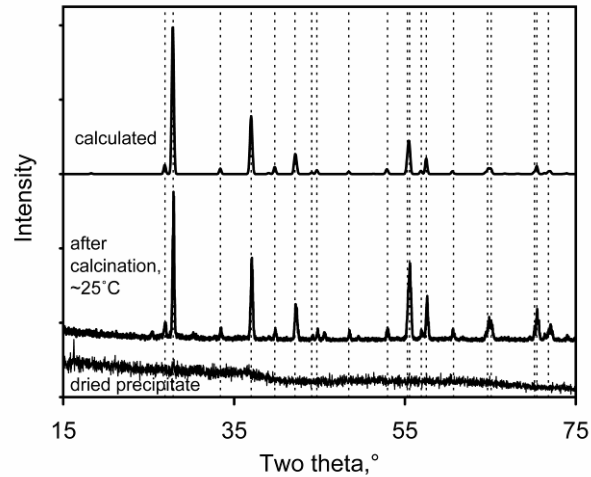
**Figure 1.** XRD patterns of $VO_2$ powder, showing pattern for $VO_2.nH_2O$ after precipitation and drying in air oven at 85°C for 1h but before heating in tube furnace (bottom), after heating in tube furnace for 20 hours at 600°C under flow of argon (centre), and the calculated pattern for $VO_2$-$M_1$ (top). Dotted lines correspond to the position of the characteristic peaks for $VO_2$-$M_1$.

*3.1.2 Ratio of $KBH_4$ to $NH_4VO_3$.* Because $KBH_4$ is easily hydrolyzed in water, it should be used over-stoichiometrically in order to keep the $NH_4VO_3$ thoroughly reduced. Table 2 shows the effect of the ratio of $KBH_4$:$NH_4VO_3$ on the products formed. Once again, the 'products' are those present in the sample after calcination at 600°C. It can be seen that $KBH_4$ could not totally reduce $NH_4VO_3$ to $VO_2$ when the ratio was less than 4. However, increased additions of $KBH_4$ also caused more of the β-$K_xV_2O_5$ to form, which is undesirable in the present context. The optimum ratio seems to be in the range of 4 to 5.

*3.1.3 Effect of pH.* As expected, the reaction proved sensitive to the pH value. Table 3 shows the effect of pH on the nature of the products. When the pH was between 4 and 5, $VO_2$-$M_1$ was obtained. $K_xV_2O_5$ was the main product obtained when the pH of the reaction was held between 5.5 and 6.5. The results are consistent with the fact that the reducing power of the $KBH_4$ decreases with an increase of the pH value.[2] In the light of these results, the pH value was kept in the range of 4 to 5 in all subsequent experiments.

*3.1.4 Effect of calcination temperature.* Figure 2 shows the DTA trace of sample #2 of table 1. The gradual weight loss of around 3% found below 190˚C is due to the release of adsorbed water. At 229˚C a broad endothermic peak is observed on the DTA curve which corresponds to the departure of chemically bound water, associated with a further 10% loss in mass. At about 320˚C and 460-480˚C there are weak exothermic peaks in the scan shown. Some other scans have a third peak at about 350˚C as well, indicating that the nature of the peaks in the range from 300 to 400˚C is variable. It is reported that $VO_2$-R crystallizes from the $VO_2$-B between 330 and 600˚C, with the lower temperature corresponding to longer times at temperature [2, 31, 37] so at least one of the peaks may be associated with this process. Gui suggests that a peak at 325˚C may correspond to the crystallization of $VO_2$-B from the amorphous precursor, and that the conversion to $VO_2$-R should be expected at a somewhat higher temperature; however both processes actually proceed over a range of temperatures [38] and neither necessarily has a fixed temperature at which it occurs. The transformation $VO_2$-B→$VO_2$-R has been found to be reconstructive in nature, and does not require long range diffusion [4]. The TGA curve is flat from 320˚C onwards, which is consistent with previous reports [31]. At 635˚C a sharp endothermic peak is observed on the DTA curve, which should correspond to the melting of any β-$K_xV_2O_5$ present [39]. It is absent in samples which lack β-$K_xV_2O_5$.
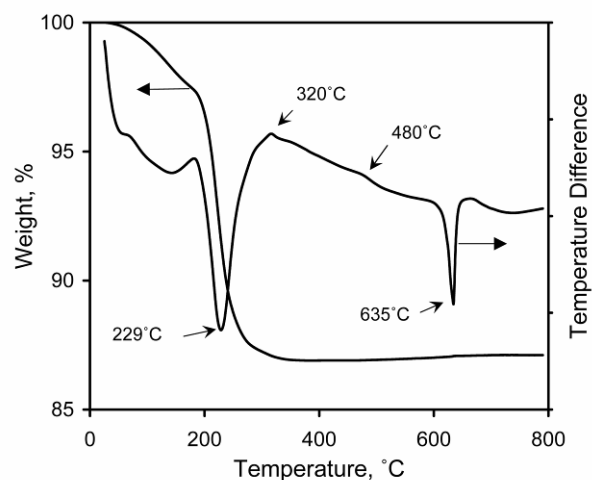
**Figure 2.** Effect of calcination. TG and DTA analysis of glycerol-free sample #2, table 1.

### 3.2 Effect of glycerol additions

*3.2.1 Increase in yield of VO$_2$.* The stoichiometry of the vanadium oxides depends strongly on the redox potential during aqueous reduction, and on the oxygen partial pressure during calcination. An attempt was made to control the latter by the addition of a small quantities of glycerol, $C_3H_5(OH)_3$, to the $NH_4VO_3$ solutions. Glycerol boils at 290˚C, and would both pyrolyse and act as a reductant at temperatures above ~400˚C. This would serve to prevent oxidation of the VO$_2$. In addition, it was hoped that there might be reduction of particle aggregation in the initial aqueous system due to the increased viscosity imparted by the glycerol. Furthermore, in the present instance, the formation of vanadium glycerate in the aqueous phase is also possible [40] and this complex, if carried over into the precipitated material, would decompose to VO$_2$.

The X-ray diffraction patterns of powder obtained with a 20% addition of glycerol are shown in figure 3. The powder that was obtained after calcining at 600˚C under a flow of Ar for 20 hours, figure 3(a), is comprised of $V_4O_7$ (JCPD card : 01-071-0423), with a minor proportion of $V_6O_{11}$ (JCPD card : 01-071-0040). There was little or no VO$_2$. Evidently the sample was over-reduced in this case, with both aqueous $KBH_4$, and the CO and H$_2$ generated during calcination, having a reductive effect. Also, the particle size of the sample was smaller than was the case when glycerol had not been added. Subsequent DTA conducted under conditions of flowing N$_2$ caused the $V_4O_7$ and $V_6O_{11}$ to be oxidized back to VO$_2$, figure 3(b). This is because the nitrogen used contained about a few ppm of O$_2$, sufficient to stabilize VO$_2$ at the expense of the lower oxides.

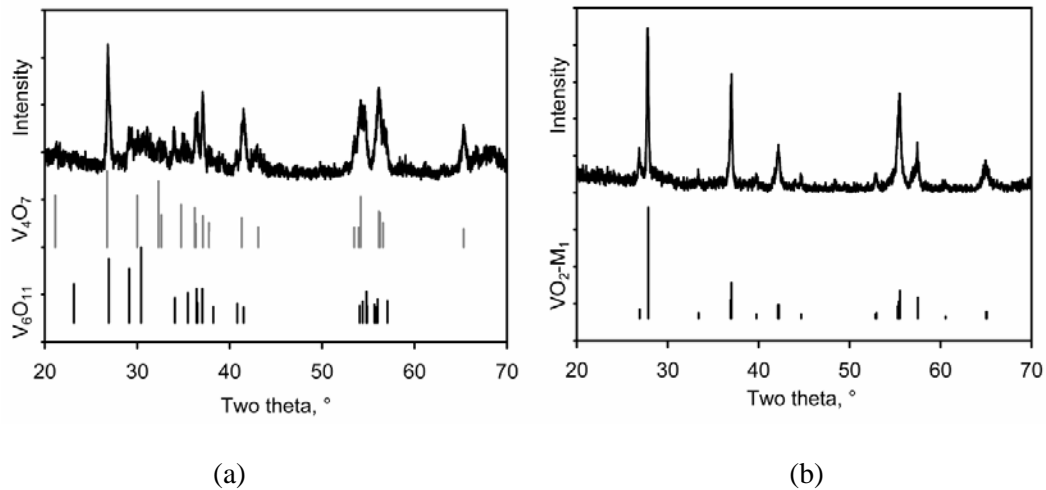(a)                                                    (b)

**Figure 3.** X ray diffraction patterns of $V_xO_y$ powders produced with additions of glycerol. (a) Tube furnace at 600˚C for 20 h under flow of Ar, (b) After DTA to 650˚C in flow of $N_2$.

*3.2.2 Effect of calcination temperature.* The temperature at which the $VO_2$-R formed under the conditions of the DTA scans was verified by sub-dividing a sample made with a 20% glycerol addition and scanning each portion to a different peak temperature, figure 4. In this sample the chemically bound water is driven off by ~290˚C, and there is an exothermic reaction between 460 and 480˚C. There is no endothermic peak at ~635˚C, indicating the absence of $\beta$-$K_xV_2O_5$ from this sample. X-ray diffraction analysis of these samples, figure 4(b), proved that it was the reaction at 460-480˚C that converted the sample to $VO_2$-R. There is no detectable $\beta$-$K_xV_2O_5$ in the X-ray patterns, as expected. There was also no evidence for $VO_2$-B, suggesting that the $VO_2$-R crystallized out of an amorphous precursor.
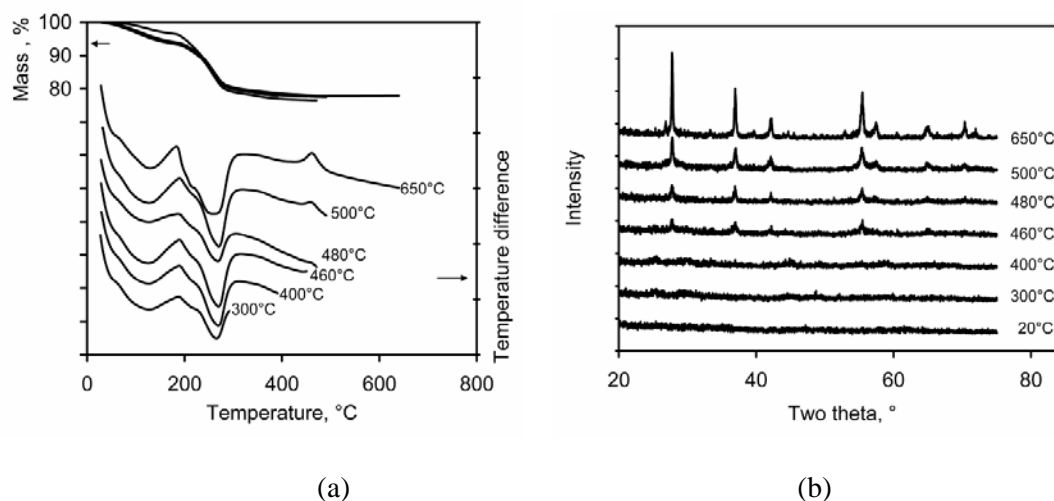
(a)  (b)

**Figure 4.**  Effect of calcination, (a) with 20% glycerol addition, scans reversed at indicated temperature (b) X-ray diffraction patterns showing effect of peak calcination.

The nature of the material produced by calcination at 300˚C and 650˚C was further investigated using TEM. In this case 40 mL of 0.25 M $NH_4VO_3$ was mixed with 8 mL glycerol and reacted with 200 mL of 0.25M $KBH_4$ at a pH of 4.1. The grain size of powder that had been calcined to 300˚C is very small, with domain sizes being of the order of 10 nm or less, figure 5. However, despite the fact that the material in this condition showed only the weakest of structure in its X-ray patterns (e.g. figure 4), it is evidently not amorphous. It not only contains a minor proportion of a non-amorphous phase (the arrowed region in figure 5 is a typical example of this type of material, which is lamellar in nature with a periodicity of the order of 0.6 to 2 nm) but furthermore, examination of the remaining (non-lamellar) material under bright and dark field conditions revealed (Fig S2, Supporting Information) that it too must possess a degree of crystallinity.
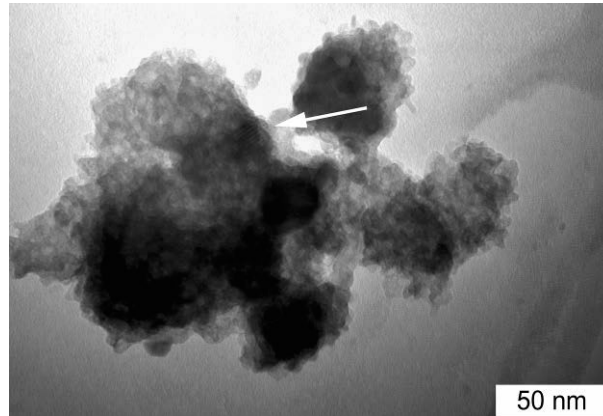
**Figure 5**. Very fine-grained material produced by calcination to 300˚C. There are regions containing a lamellar phase (arrowed).

Material that had been calcined to 650˚C and cooled to room temperature appeared fully crystalline, as expected from the corresponding X-ray patterns. TEM examination revealed that the samples consisted of polygonal crystals, between 30 and 100 nm in width, figure 6 (see also Fig S3, Supporting Information). Sub-structure was visible in the $VO_2$-$M_1$ grains and these linear features have been previously identified in the literature as 'dislocations' [37]. However, by analogy to the structures produced in other (metallic) displacively-transforming systems e.g.[41, 42] it is more reasonable to identify them as 'laths'. The laths correspond to individual domains of the monoclinic phase, while the lamellar structures may be microtwinned domains formed by adaptive twinning driven by the elastic stresses of the transformation, see for example [43]. The periodicity of these features varied between 0.6 and 2.0 nm, the same as those noted earlier in the material calcined to only 300˚C. Since, X-ray diffraction of the present sample indicated only $VO_2$-$M_1$, it is probable that the lamellar regions noted in figure 5 were also $VO_2$-$M_1$, but present in insufficient volume to appear on the X ray diffraction pattern.
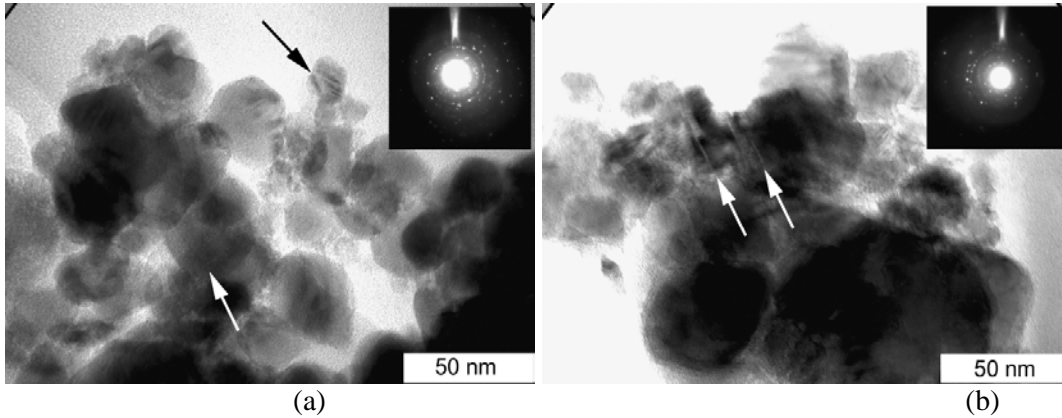
(a)                                                          (b)

**Figure 6.** TEM images and global electron diffraction patterns of material that had been calcined to 650˚C and then transformed to $VO_2$-$M_1$ on being cooled to room temperature. (a) Laths (arrowed) formed by the displacive transformation $VO_2$-$R\rightarrow VO_2$-$M_1$. (b) Twinning and microtwinning (arrowed) in the $VO_2$-$M_1$ microstructure. (Electron diffraction patterns are shown at half the magnification of the TEM images.)

*3.3 Optimum material*

$VO_2$-R could be reliably produced if the pH of the reaction was held at about 4.2, the ratio of $KBH_4$ to $NH_4VO_3$ was 5, 20% by volume of glycerol was added to the $NH_4VO_3$, the temperature of the reaction was between 20 to 25˚C, the samples were air dried at 85˚C, and calcination was carried out at 600˚C for several hours under an inert gas. Under these conditions the resulting material is almost pure, and has an XRD pattern nearly identical to the standard pattern in JCPDS card : 44-0252. Figure 7 shows that the diameter of the $VO_2$ particles produced by calcination in the presence of glycerol additions is about 100 to 300 nm. The diameter of these particles is larger than those shown in the TEM images, due evidently to sampling issues.
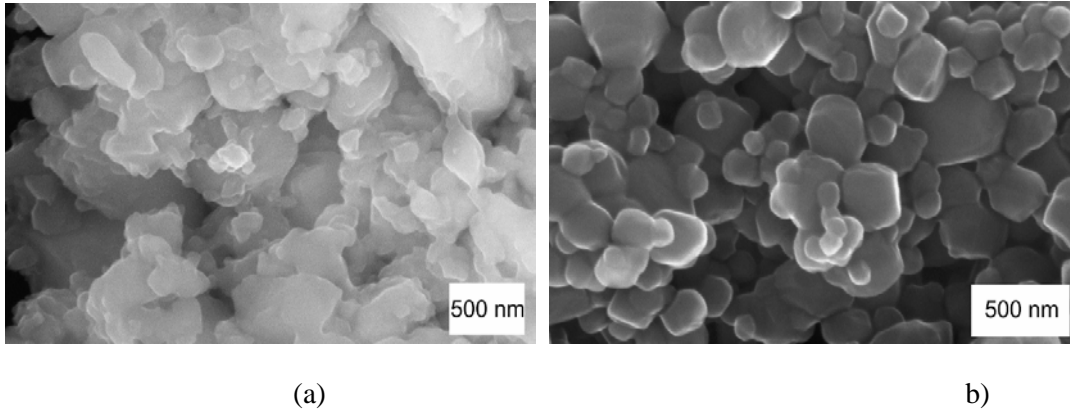
(a)          b)

**Figure 7.** SEM photos of $VO_2$ nano-particles produced as described in the text. (a) After drying at 85°C for 3 hours, (b) after calcination at 600°C in the DTA apparatus.

The reversibility of the metal insulator transformation was examined using differential scanning calorimetry [44] and X-ray diffraction (Fig S4, S5 and S6, Supporting Information). In the un-doped material the $VO_2$-$M_1$ was transformed to $VO_2$-R at 66°C, which is within the range of the temperatures reported for this phenomenon. There was an exothermic peak at 61°C during cooling down, corresponding to $VO_2$-R→$VO_2$-$M_1$. Doping with Mo brought the up and down transformation temperatures to 59.6 and 54.7ºC respectively, while doping with W moved them to 59.2 and 57.3ºC. The Mo and W content in the doped material was determined to be of the order of 0.70 and 0.15 at.% respectively. The hysteresis 5K or so is characteristic of 'bulk $VO_2$, or at least of $VO_2$ with an abundance of sites at which nucleation can occur[20].

**3.4 Optical properties of $VO_2$-containing coatings**

The optical properties of $VO_2$ are summarized in figure 8. The refractive indices of $VO_2$-$M_1$ and $VO_2$-R thin films are shown in figure 8(a), with data from Verleur [36] and from our own work on continuous thin films [17] for comparison. $VO_2$-R can be seen to become plasmonic when its $n$ and $k$ curves cross near 1 μm .The optical extinction properties of $VO_2$ *nanoparticles* are controlled by two rather different phenomena : scattering and absorption, with both strongly influenced by the plasmon resonance, if there is one. Plasmon resonance is expected when $n^2 - k^2 (= \varepsilon_1) \approx -2$, and this occurs in

the near-infrared for $VO_2$-R but not at all for $VO_2$-$M_1$. Scattering is far less important than absorption in very small $VO_2$ particles (<100 nm) but becomes significant as the particle size increases beyond that. Whereas absorption is an important consideration is transmissive coatings, it is scattering that is most important when $VO_2$ nanoparticles are used as an opaque pigment, since this is the only mechanism by which they can modulate energy flux off the coating. The optical scattering efficiencies of a range of target shapes (figure 8b) were calculated here using Mie theory (possible for spheres) and the discrete dipole approximation (DDA, possible for any sufficiently small shape) (figure 8c). All targets contained the same volume of $VO_2$, that of a sphere of 200 nm radius. The porous aggregate of irregularly-shaped crystals had an average packing density of 38%. In all three cases scattering of the $VO_2$-R peaked in the near-infrared due to a broad plasmon resonance at about 1.4 μm, whereas that of $VO_2$-$M_1$ has a peak centered near 1.2 μm. This $VO_2$-$M_1$ peak is linked to excitation of carriers across the band gap between the valence and conduction bands of the semiconductor. The plasmon resonance peak for the aggregate and cubes is slightly broader than for the spheres but is otherwise located at a similar wavelength. Therefore, we submit that, as a first approximation, it is feasible to use Mie theory calculations of the optical properties of spheres as a way of exploring the possibilities of $VO_2$ nanocrystal coatings. This is convenient as the analytical solutions are not only very much faster, but can also be scaled up to particle sizes that exceed the capability of the DDA method.
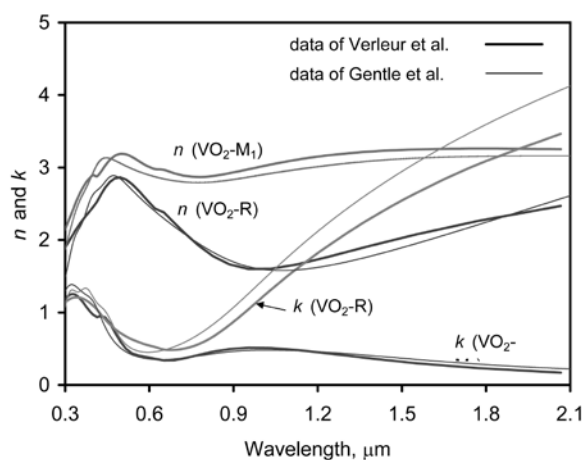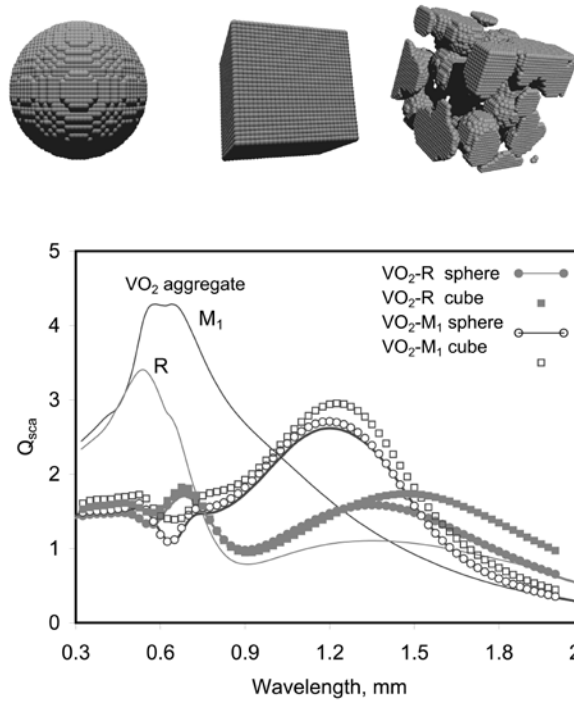
**Figure 8**. Optical properties of vanadium dioxide films and nanoparticles. (a) Refractive index data for VO$_2$-R and VO$_2$-M$_1$ determined by the authors and obtained from the literature. (b) Representations of the three types of VO$_2$ targets used here in simulations of optical properties. Each little sphere corresponds to an active dipole in the DDA model. (c) Calculated optical extinction efficiencies of 200 nm radius VO$_2$ spheres, cubes and a porous aggregate, all in vacuum and all containing the same volume of VO$_2$. The symbols correspond to DDA calculations and the lines to Mie theory calculations. Simulations of the light scattered off spherical VO$_2$ nanoparticles of various diameters are shown in figure 9, and are compared to measurements made of two glass slides coated with an opaque layer of VO$_2$ powder. Some broad trends are obvious, especially when a comparison is made to the measured data. In particular, the relative scattering efficiencies of VO$_2$-M$_1$ and -R spheres inverts several times in the visible and near-infrared part of the spectrum, as size and $\lambda$ are varied. In general however, when $r<300$ nm, it is the semi-conducting VO$_2$-M$_1$ phase that scatters more strongly. The VO$_2$-R particles in general only become better scatterers when $r>300$ nm, and then only for $\lambda>1$ $\mu$m.
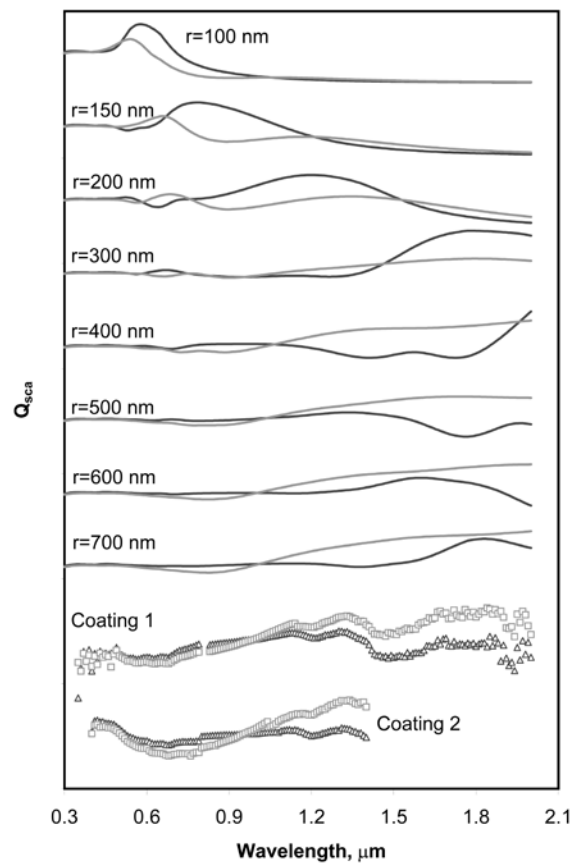
**Figure 9.** Calculated scattering efficiencies of $VO_2$-$M_1$ (dark) and $VO_2$-R (light) cubes of indicated effective radius, compared to measured data for reflectivity for two sample coatings with same color coding.

More insight into the situation may be gained by defining a wavelength-dependent switching ratio, $\beta(\lambda) = Q_{sca}(\lambda) \ VO_2$-R $/ Q_{sca}(\lambda) \ VO_2$-$M_1$ which provides a useful figure-of-merit. In general, the higher $\beta$ the greater the degree of switching expected at the given wavelength. If $\beta > 1$ then the $VO_2$-R phase will scatter more than the $VO_2$-$M_1$, and conversely for $\beta < 1$ it is the $VO_2$-$M_1$ phase that is the better scatterer. The ratios of light scattered off the experimental coatings are plotted in Fig 10a against $\beta(\lambda)$ data calculated for a mixture of spherical $VO_2$ nanocrystals of the indicated sizes. The congruence of the measured and calculated data is excellent, given the many variables in this system. It is clear, that the measured data are in congruence with an effective $VO_2$ particle size in the range of 500 to 800 nm radius.

The advantage of the numerical technique is that it also permits exploration of morphologies that have not yet been produced. For example, in Figure 10b we show that the figure-of-merit for porous aggregates of $VO_2$ crystals of the indicated effective radius would be even better than that of cubes.
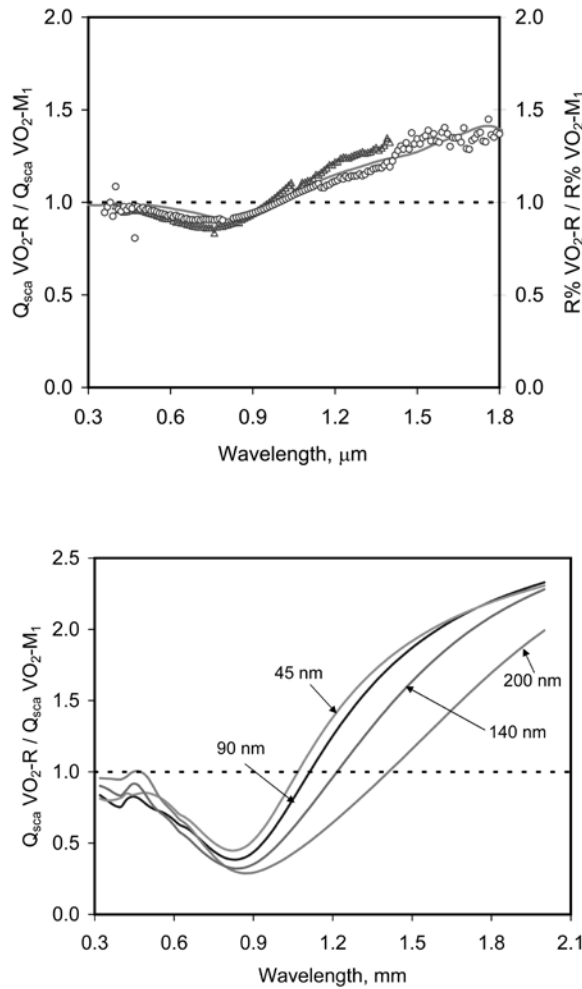


**Figure 10.** (a) Ratio of light scattered off high and low temperature states of experimental coatings of $VO_2$ as a function of wavelength (symbols), compared to ratio of $Q_{sca}$ $VO_2$-R to $Q_{sca}$ $VO_2$-$M_1$ calculated for a mixture of $VO_2$ spheres (solid line). (The mixture is somewhat arbitrarily composed of 22% each of 500, 600 and 700 nm radius spheres, plus 35% of 800 nm diameter spheres. This is not necessarily the only mixture of $VO_2$ spheres that could simulate the measured data). Note the similarity in magnitude and shape of the measured and calculated data sets. (b) Ratio of $Q_{sca}$ $VO_2$-R to $Q_{sca}$ $VO_2$-$M_1$ calculated for porous aggregates of $VO_2$ nanocrystals having a 38% volume fraction of $VO_2$.

It is obviously of interest to try establish the optimum shape and size of $VO_2$ nanoparticle to maximize the switching effect in these coatings. We have seen from figure 8 that aggregation of individual $VO_2$

particles broadens the plasmon resonance further into the infrared, and this is a desirable outcome in the present context. For maximum heat rejection on hot days its is desirable that $\beta>1$ over as much of the spectrum as possible so that the coating stays cool. This broadening of the plasmon resonance peak also smoothed out or eliminated the reversals in scattering efficiency that occurred as wavelength varied for the spheres and cubes (e.g. figure 9). Alternatively, the peak can also be broadened by using a mixture of $VO_2$ particles of different sizes. Interestingly, the opposite effect (having $\beta<1$) will tend to *increase* temperature fluctuations in the coating. This is because such coatings will scatter a greater proportion of the incoming radiation when cold than when hot, all else being equal.

The experimental coatings show a relative variation of about 30% in their measured reflectivity over the range 1.5 to 1.8 $\mu$m, but are in general rather dark and absorptive due to a rough surface topography [25]. Nevertheless, these results indicate that further development of these pigments will be possible if their switching contrast can be raised. It is evident from figures 8 and 9 that the optical properties of $VO_2$ coatings do not change much in the visible part of the spectrum. The greatest modulation is in the near-infrared and, in the case of coatings comprised of nanoparticles, is associated with the appearance and disappearance of the localized surface plasmon resonance at about 1500 nm. For this reason the modulation of the optical properties of the nanoparticle-based systems are qualitatively and quantitatively rather different from those of smooth films of $VO_2$.

## 4. Conclusions

A convenient wet chemical process to synthesize $VO_2$-$M_1$ by reductive-precipitation of $NH_4VO_3$ using $KBH_4$ and glycerol, followed by filtering, washing and calcination, is described. The addition of the glycerol to the starting solutions significantly improves quality of the $VO_2$ product. Nanocrystalline aggregates of tabular $VO_2$ were produced which were characterized and incorporated into simple coatings. Unlike the case in continuous thin films of $VO_2$, the switchable optical properties of such particulate material was controlled by a near-infrared plasmon resonance in the $VO_2$. A significant intensity of switching in optical absorption efficiencies is theoretically predicted in the near-infrared, with the effect somewhat stronger for aggregates than for nanospheres. However, the actual switching observed in the samples was only of the order of 30%, expressed as one phase relative to the other. In any case, both $VO_2$-$M_1$ and $VO_2$-R are fundamentally dark-colored pigments, and therefore can only be used to modulate the near-infrared properties of coatings that are already quite absorptive anyway.

## References

[1]     Livage, J. 1999 *Coordin. Chem. Rev.* **190-192** 391.
[2]     Tsang, C. F., Kim, J. and Manthiram, A. 1998 *J. Mater. Chem.* **8**(2) 425.
[3]     Soltani, M., Chaker, M., Haddad, E. and Kruzelesky, R. 2006 *Measurement Science and Technology* **17** 1052.
[4]     Leroux, C. and Nihoul, G. 1998 *Phys. Rev. B* **57**(9) 5111.
[5]     Morin, F. J. 1959 *Phys. Rev. Lett.* **3**(1) 34.
[6]     Nag, J. and Haglund, R. F. J. 2008 *J. Phys.: Condens. Matter* **20** 264016.
[7]     Shi, J., Zhou, S., You, B. and Wu, L. 2007 *Solar Energy Materials & Solar Cells* **91** 1856.
[8]     Mlyuka, N. R. and Kivaisi, R. T. 2006 *J. Mater. Sci.* **41** 5619.
[9]     Manning, T. D. and Parkin, I. P. 2004 *Journal of Materials Chemistry* **14** 2554.
[10]    Hanlon, T. J., Coath, J. A. and Richardson, M. A. 2003 *Thin Solid Films* **436** 269.
[11]    He, J., Lin, L.-b., Lu, Y., Lu, T.-c., Liu, Z.-h. and Wang, J. 2005 Electrical and optical properties of $VO_2$ thin films affected by preparation process, *Device and Process Technologies for Microelectronics, MEMS, and Photonics IV*, Brisbane, Australia, J.-C. Chiao, A. S. Dzurak, C. Jagadish, D. V. Thiel (eds.), p. 60371K.

[12]     Choi, H. S., Ahn, J. S., Jung, J. H., Noh, T. W. and Kim, D. H. 1996 *Phys. Rev. B* **54**(7) 4621.

[13]     Xiao, D., Kim, K. W. and Zavada, J. M. 2005 *J. Appl. Phys.* **97** 106102.

[14]     Karakurt, I., Boneberg, J., Leiderer, P., Lopez, R., Halabica, A. and R. F. Haglund, J. 2007 *Appl. Phys. Lett.* **91** 091907.

[15]     MacChesney, J. B. and Guggenheim, H. J. 1969 *J. Phys. Chem. Solids* **30** 225.

[16]     Biermann, S., Poteryaev, A., Lichtenstein, A. I. and Georges, A. 2005 *Phys. Rev. Lett.* **94** 026404

[17]     Gentle, A., Maaroof, A. I. and Smith, G. B. 2007 *Nanotechnology* **18**(2) 025202.

[18]     Kakiuchida, H., Jin, P. and Tazawa, M. 2008 *Solar Energy Materials & Solar Cells* **92** 1279.

[19]     Jin, P., Xu, G., Tazawa, M. and Yoshimura, K. 2003 *Applied Physics A. Materials Science & Processing* **77** 455.

[20]     Lopez, R., Haynes, T. E., Boatner, L. A., Feldman, L. C. and Haglund, R. F. 2002 *Phys. Rev. B* **65** 224113.

[21]     Lopez, R., Haynes, T. E., Boatner, L. A., Feldman, L. C. and R. F. Haglund, J. 2002 *Opt. Lett.* **27**(15) 1327.

[22]     Rini, M., Cavalleri, A., Schoenlein, R. W., López, R., Feldman, L. C., Richard F. Haglund, J., Boatner, L. A. and Haynes, T. E. 2005 *Opt. Lett.* **30**(5) 558.

[23]     Guinneton, F., Valmalette, J.-C. and Gavarri, J.-R. 2000 *Optical Materials* **15** 111.

[24]     Valmalette, J. C. and Gavarri, J. R. 1994 *Solar Energy Materials and Solar Cells* **33** 135.

[25]     Guinneton, F., Sauques, L., Valmalette, J.-C., Cros, F. and Gavarri, J.-R. 2005 *J. Phys. Chem. Solids* **66** 63.

[26]     Bianconi, A., Stizza, S. and Bernardini, R. 1981 *Phys. Rev. B* **24**(8) 4406.

[27]     Cortie, M. B., Dowd, A., Harris, N. and Ford, M. J. 2007 *Phys. Rev. B* **75** 113405.

[28]     Cortie, M. B., Barnett, M. W. and Ford, M. J., in *SPIE Optics and Photonics Conference*, San Diego, California, USA **2007**.

[29]     Mikheeva, O. P. and Sidorov, A. I. 2003 *Technical Physics* **48**(5) 602.

[30]     Manivannan, V. and Goodenough, J. B. 1998 *Materials Research Bulletin* **33**(9) 1353.

[31]     Gui, Z., Fan, R., Mo, W., Chen, X., Yang, L., Zhang, S., Hu, Y., Wang, Z. and Fan, W. 2002 *Chem. Mater.* **14** 5053.

[32]     Bohren, C. F. and Huffman, D. R. 1998 *Absorption and Scattering of Light by Small Particles*, (New York: Wiley).

[33]     Laven, P. 2006, *MiePlot. A computer program for scattering of light from a sphere using Mie theory & the Debye series*, http://www.philiplaven.com/mieplot.htm, accessed 10th April 2007.

[34]     Draine, B. T. and Flatau, P. J. 1994 *J. Opt. Soc. Am. A* **11**(4) 1491.

[35]     Draine, B. T. and Flatau, P. J. 2004, *User Guide for the Discrete Dipole Approximation Code DDSCAT 6.1*, http://arxiv.org/abs/astro-ph/0309069, accessed 10th January 2007.

[36]     Verleur, H. W., Barker, A. S. and Berglund, C. N. 1968 *Physical Review* **172**(3) 788.

[37]     Sahana, M., Subbanna, G. and Shivashankar, S. 2002 *J. Appl. Phys.* **92**(11) 6495.

[38]     Gui, Z., Fan, R., Chen, X. H. and Wu, Y. C. 2001 *Journal of Solid State Chemistry* **157** 250.

[39]     Maingot, S., Baffier, N., Pereira-Ramos, J. P. and Willmann, P. 1993 *Solid State Ionics* **67** 29.

[40]     Tracey, A. S., Gresser, M. J. and Parkinson, K. M. 1987 *Inorg. Chem.* **26**(5) 629.

[41]     Porter, D. A. and Easterling, K. E. 1992 *Phase Transformations in Metals and Alloys*, (Boca Raton: Taylor and Francis).

[42]    Cortie, M. B. and Levey, F. C. 2002 *Intermetallics* **10** 23.

[43]    Khachaturyan, A. G., Shapiro, S. M. and Semenovskaya, A. 1991 *Phys. Rev. B* **43**(13) 10832.

[44]    Bai, H., Berkahn, M. and Cortie, M. B.,  2007, 31st Annual Condensed Matter and Materials Meeting, http://www.aip.org.au/wagga2007/2007_3.pdf, Australian Institute of Physics, Melbourne, accessed 23rd May 2007.

**Table 1.** Effect of reaction temperature on composition of products.

| T(˚C) | Products(XRD results) |
|---|---|
| 0 | $VO_2$-$M_1$+ β-$K_xV_2O_5$ |
| 25 | $VO_2$-$M_1$+ β-$K_xV_2O_5$ |
| 40 | $VO_2$-$M_1$+$V_6O_{13}$+ β-$K_xV_2O_5$ |
| 70 | β-$K_xV_2O_5$ |

**Table 2.** Effect of the ratio of $KBH_4$:$NH_4VO_3$ on composition of products.

| $KBH_4$ : $NH_4VO_3$ | Products(XRD results) |
|---|---|
| 1.5 | $V_2O_5$ |
| 2 | $V_2O_5$ |
| 3 | $VO_2$-$M_1$+$V_6O_{13}$+ β-$K_xV_2O_5$ |
| 4 | $VO_2$-$M_1$+ β-$K_xV_2O_5$ |
| 5 | $VO_2$-$M_1$+ β-$K_xV_2O_5$ |

**Table 3.** Effect of pH value on composition of products.

| pH | Products(XRD results) |
|---|---|
| <4 | Transparent blue-black solution |
| 4~5 | $VO_2$-$M_1$+ β-$K_xV_2O_5$ |
| 5.5 | $VO_2$-$M_1$ + β-$K_xV_2O_5$ |
| 6.5 | β-$K_xV_2O_5$ |

**Supporting Information**



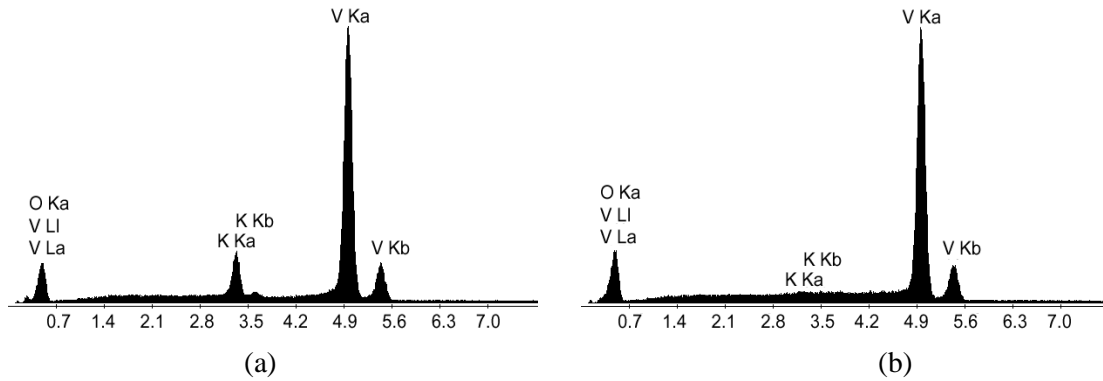(a)                                                         (b)

**Figure S1.** The presence of the $\beta$-$K_xV_2O_5$ was also indicated by a peak for K when electron dispersive spectroscopy was performed on the powder samples. (a) $VO_2$ sample containing $\beta$-$K_xV_2O_5$, produced at a pH of ~4.5, (b) Sample produced at a pH of ~4.3 and thoroughly washed with warm water and methanol.
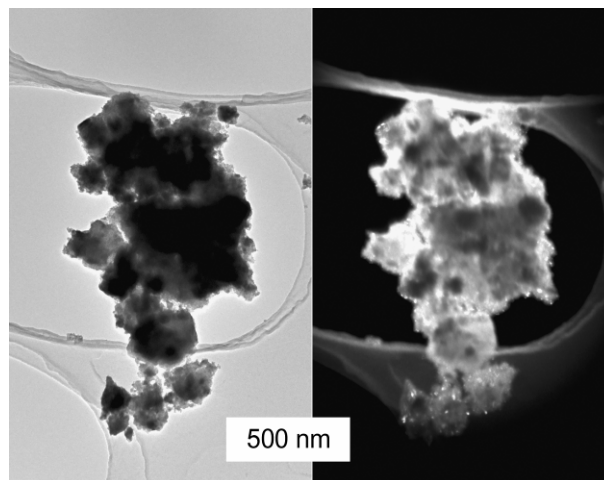


**Figure S2.** Bright and dark field imaging of a particle of powder produced by calcining to 300˚C. The bright spots in the dark field image are individual grains with orientations that match the orientation selected by the microscopist. Note, however, that the overall diffuse white glow is due to electron scattering by amorphous material).
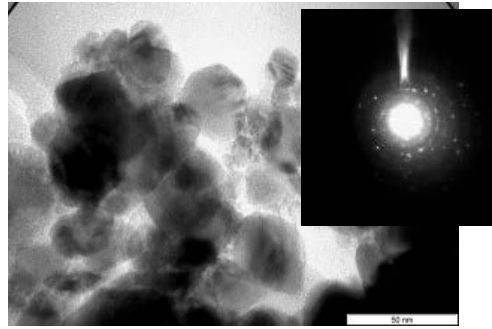
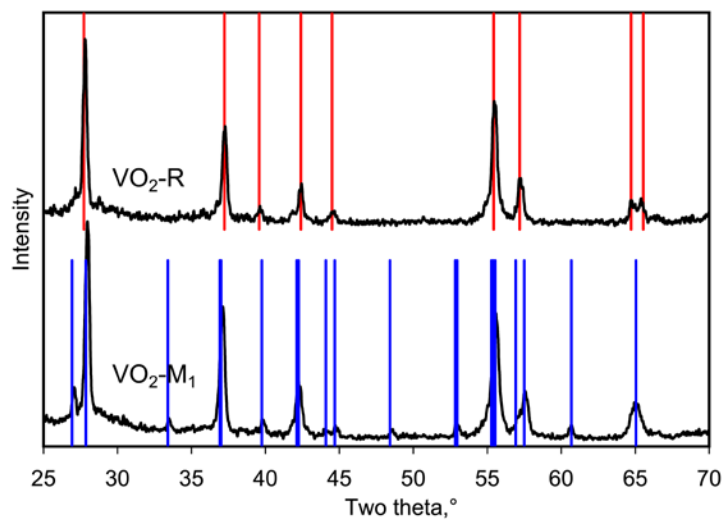**Figure S3** TEM image and global electron diffraction pattern of VO$_2$ nanoparticles



**Figure S4** XRD patterns of VO$_2$-M$_1$ at room temperature and VO$_2$-R at ~80˚C, monitored using in situ X-ray diffraction. It can be seen that the synthesized VO$_2$ is almost pure, and has a different XRD pattern at low temperature and high temperature. These are nearly identical to the standard patterns of JCPDS 44-0252 (VO$_2$-M, blue lines) and 01-073-2362 (VO$_2$-R, red lines), respectively.
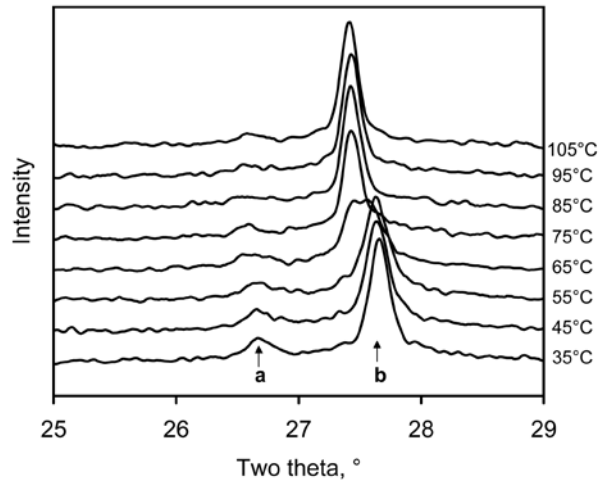
**Figure S5** XRD patterns in the 2θ interval of 25 to 29°, taken at successively higher temperatures, showing the disappearance of the peaks (*a* and *b*) of $VO_2$-$M_1$ and the appearance of a prominent one for $VO_2$-R. There is an intermediate region in which the two phases co-exist.
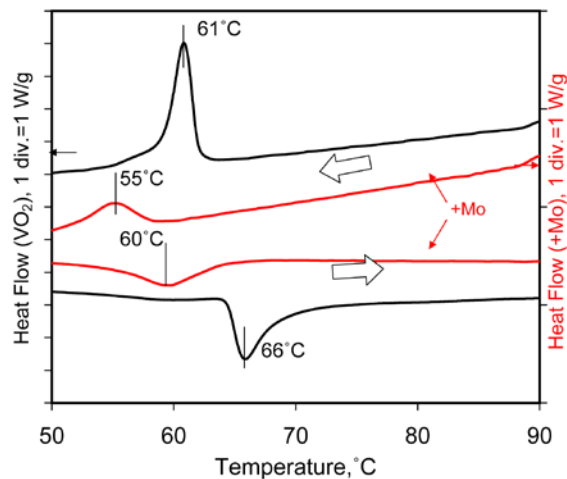


**Figure S6** DSC curves of un-doped (left-hand axis) and Mo-doped (right-hand axis) $VO_2$, showing the reversibility of the metal-insulator transformation and characteristic hysteresis. It can be seen that $VO_2$-$M_1$ was transformed to $VO_2$-R at 66°C while the reverse reaction occurred at about 61°C during cooling. After doping with Mo the phase transmission temperatures decreased to 60°C and 55°C respectively. Analysis by EDS showed that the ratio of Mo/V was only 0.7 atom %, so a greater amount of doping by the method used seems feasible if required.